Development of a Small-Scale Aeroelastic Apparatus for Limit Cycle Oscillation Data Collection

Avaneesh Ravat* and Matthew Bryant†
North Carolina State University, Raleigh, North Carolina 27606

As aircraft structures interact with their surroundings, they are subject to aerodynamic, elastic, and inertial forces. The interaction of these forces can cause deformations, vibrations, and in extreme cases, limit cycle oscillations (LCO), a nonlinear dynamic phenomenon characterized by a system's self-sustained cyclic oscillation between two amplitude limits at a constant frequency. These oscillations can, over time, risk structural damage and loss of control. These risks are amplified when dealing with a system that experiences LCO as a result of a subcritical Hopf bifurcation for two reasons. Firstly, the onset of LCO can occur below the critical flight parameter (linear flutter airspeed in aeroelastic systems) if the system is excited beyond an unstable amplitude boundary. Secondly, the system exhibits a jump instability at the critical flight parameter where the system abruptly changes from zero oscillations to high-amplitude LCO. Due to these risks, it is desirable to be able to predict and prevent the onset of LCO, however, sources of nonlinearity, including but not limited to structural nonlinear stiffness and damping terms, coupling between the system's degrees-of-freedom (DOF), and phenomenon like dynamic stall, make this difficult to achieve analytically. Therefore, empirical techniques are of interest. A common empirical method is to fit the Hopf Amplitude Equation to data collected from the system of interest. This equation, however, loses accuracy at flight parameter values far from the critical flight parameter. Machine learning techniques have been proposed as a means of empirically predicting the onset of LCO in systems that experience subcritical Hopf bifurcations, however, these models require large amounts of data for training. In this paper, a two DOF wind tunnel apparatus is developed in order to generate this training data. This apparatus is designed to enter LCO in a small-scale wind tunnel (0.28 x 0.28 m) with maximum wind speeds of 15 m/s. This apparatus has a pitch DOF, supported by linear springs, and a heave DOF, supported by spring steel beams. Different airfoils, each 0.24 m tall, are 3D printed for use in the apparatus and can easily be swapped to help generate a more diverse dataset. Collecting data on different airfoils may help the machine learning model separate patterns unique to each airfoil from key generalizations about the true dynamics of LCO. Additionally, the entire apparatus is mounted to an extruded aluminum frame, allowing for quick mounting and dismounting to the wind tunnel. This work lays the foundation for future improvements to the apparatus.

I. Introduction

Aircrafts, among other structures and bodies, are subject to many forces. Interactions with surrounding fluids result in aerodynamic forces, structural flexibilities contribute to elastic forces, and inherent properties of the aircraft, such as mass, lead to inertial forces. The static and dynamic response of an elastic body to the interaction of these forces defines aeroelasticity [1].

A possible response to these forces is a phenomenon known as flutter, which is characterized by self-excited oscillations commonly occurring in the aircraft's wing or horizontal stabilizer. Flutter is caused by deformations in the flexible components of aircrafts. These deformations, along with added energy from airflow and insufficient damping, result in the observed oscillations [2]. Flutter is traditionally predicted using linear dynamic models, which identify a flutter boundary - a critical condition, such as wind speed or dynamic pressure, where the aircraft becomes dynamically unstable [3]. At conditions above the flutter boundary, linear models predict that the oscillations will grow exponentially. However, in reality, this is not the case for aeroelastic systems because of nonlinear effects, which limit the growing oscillation amplitude. Sources of nonlinearities include unsteady aerodynamics, structural nonlinearities,

*Undergraduate Student, Department of Mechanical and Aerospace Engineering, 1840 Entrepreneur Drive, Raleigh, NC 27606, Student Member
†Professor, Department of Mechanical and Aerospace Engineering, 1840 Entrepreneur Drive, Raleigh, NC 27606

and nonlinear stiffnesses [4]. These nonlinear effects result in self-sustaining, constant amplitude oscillations, a state known as limit-cycle oscillation (LCO). One such system that experiences LCO is a system capable of experiencing a Hopf bifurcation. Hopf bifurcations can be categorized into supercritical and subcritical bifurcations. For LCO in systems experiencing supercritical Hopf bifurcations, the oscillation amplitude increases with increasing wind speeds beyond the critical wind speed. At conditions below the critical wind speed, disturbances die out. However, in systems experiencing subcritical Hopf bifurcations, LCO can still occur below the critical wind speed. In this subcritical range, the steady state behavior of the aeroelastic system is dependent on the magnitude of the initial oscillation of the system due to the existence of an unstable boundary [5]. If the initial oscillation amplitude exceeds the unstable boundary, the system will enter stable LCO. These characteristics of subcritical Hopf bifurcations make it difficult to predict whether a given disturbance will result in LCO.

LCO in aircrafts, especially in systems that experience subcritical Hopf bifurcations, is undesirable because repeated oscillations cause fatigue in structures and loss of control [6]. Therefore, it is desirable to annihilate LCO or take the appropriate action to prevent LCO from occurring if it is impending. Current efforts focus on implementing flutter constraints during the design optimization process [6] and developing control strategies to deploy mechanical actuators [7] and piezoelectric actuators [8]. Existing literature developed by the Intelligent Structures and Systems Research Lab (ISSRL) at North Carolina State University (NCSU) has detailed the potential benefits of utilizing machine learning techniques, specifically recurrent neural networks (RNNs), to predict whether an aeroelastic system will enter LCO [9],[10]. Due to developments in mathematical and physics-based models of LCO [11],[12],[13], physics-informed neural networks (PINNs) are of interest. They have the ability to combine relevant, known physics relationships with underlying patterns not captured by traditional dynamic models [14]. To develop reliable models, machine learning algorithms require tremendous amounts of data. As a result, it is of interest to develop an apparatus capable of being excited into LCO that is readily available to generate data. In this work, the development of such an apparatus is detailed, including the design, fabrication, and evaluation of the design.

II. Methodology

A. Previous Work and Proposed Solutions

The ISSRL lab has developed a two degree-of–freedom apparatus to excite into a state of LCO in the NCSU Subsonic Wind Tunnel [9]. A challenge with this large-scale apparatus is ease of assembly - with many parts to assemble, it is time consuming to correctly put everything together in the wind tunnel. Also, with other labs requiring wind tunnel access, the ISSRL lab has limited time to collect data. Additionally, the fabrication of airfoils that are compatible with this apparatus requires extensive manufacturing techniques.

To avoid schedule conflicts with other labs, this new apparatus will be designed for the small-scale wind tunnel located in the ISSRL lab, shown in Fig. 1. The development of a new apparatus aims to address these other challenges by (1) creating a way to easily mount and dismount the apparatus from the wind tunnel and (2) being compatible with 3D printed airfoils. Additionally, this small-scale apparatus should allow new 3D printed airfoils to easily be attached to and removed from the apparatus.

B. Design Considerations

The size of the test section's opening is 0.28 m x 0.28 m (11 in x 11 in). The apparatus is mounted to the aluminum extrusions running vertically on the opening of the wind tunnel, as depicted in Fig. 2. The wing should be the only component that spans the test section; connecting hardware and extraneous components should be as minimally invasive to the test section as possible to limit potential nebulous aerodynamic effects. Using a P1S 3D printer manufactured by Bambu Lab, a decambered SD7003 airfoil with a height of 0.24 m (9.5 in) and chord length of 0.060 m (2.375 in) was printed. This airfoil matches the airfoil used in the large-scale setup and was dimensioned such that it maintained the large-scale airfoil's aspect ratio of four [9]. Elliptical plates were added to the ends of the airfoil. These plates help minimize the formation of vortices at the wing tips, therefore mimicking 2D flow [15]. The leading edge of the airfoil faces the wind tunnel opening.

The apparatus has two degrees-of-freedom (DOF): heave and pitch. Heave displacement is measured using a laser vibrometer. Pitch rotation is measured using an optical encoder manufactured by US Digital (Version E6).

In addition, this apparatus is expected to endure violent oscillations throughout its useful lifetime. Therefore, it was built with durability in mind - components that could loosen or wear out over time were avoided.

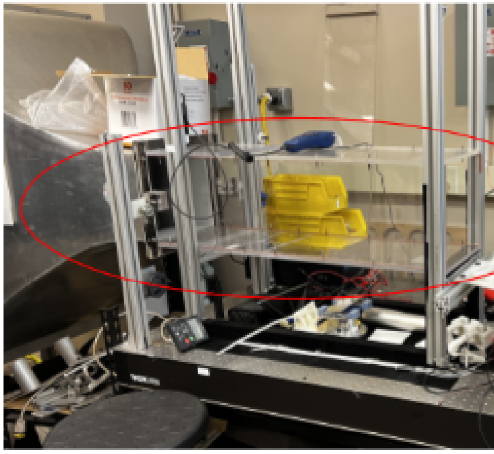

Fig. 1 The small-scale wind tunnel located in the ISSRL laboratory

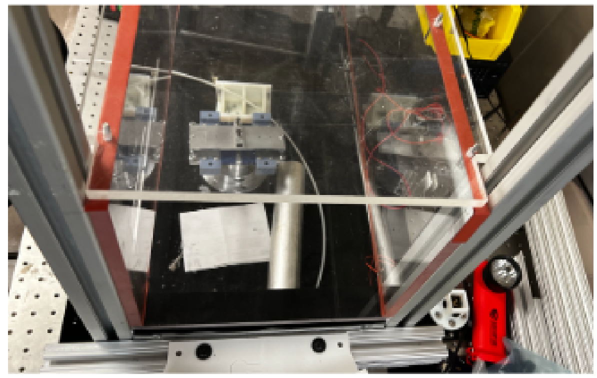

Fig. 2 Test section opening

C. Design Overview

The design of this apparatus is shown in Fig. 3 and 4. It is modeled in SolidWorks.

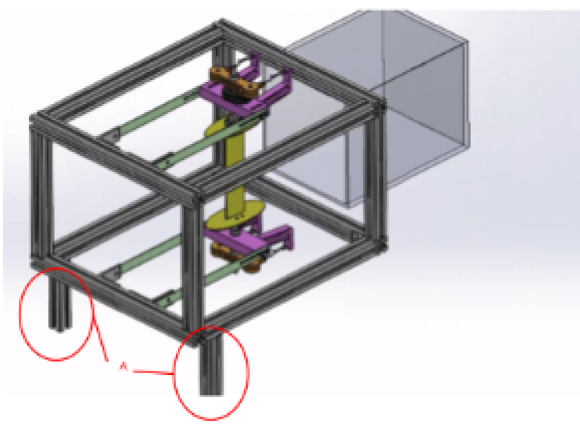

Fig. 3 Design of the apparatus

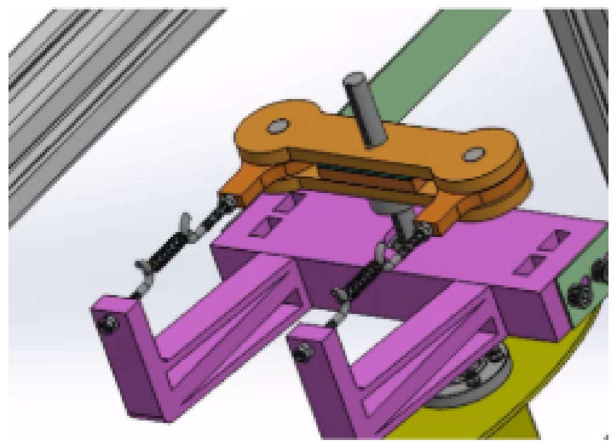

Fig. 4 Location of linear springs

The apparatus is mounted to the wind tunnel via a cage made of aluminum extrusions. Using 80/20 Aluminum brackets, this cage can be attached to the vertical extrusions on the wind tunnel. The entire apparatus is then attached to this cage via four spring steel beams (shown in green in Fig. 3). This arrangement allows quick mounting and dismounting of the apparatus from the wind tunnel without having to disassemble any parts. The two extrusion pieces labeled A in Fig. 3 are placed to support the apparatus - without them, the apparatus would be cantilevered. These pieces are offset from the end of the cage to align with mounting holes on the table beneath the wind tunnel (see table in Fig. 2).

Stiffness in the heave DOF is provided by thin, flexible spring steel beams (depicted in green in Fig. 3 and 4), which act as fixed-guided beams. There are two beams at the top and two beams at the bottom of the apparatus. Each beam is 0.38 m (15 in) long and 0.025 m (1 in) wide. One end was mounted to the aluminum extrusions via the mounting bracket and the other end was attached to the wing heave mount (shown in pink in Fig. 4).

Stiffness in the pitch DOF is given by four linear springs - two at the top and two at the bottom. The location of these springs is shown in Fig. 4.

The airfoil is depicted in yellow. As seen in Fig. 5, the airfoil takes up the majority of the test section opening. Additionally, mounting the spring steel beams to the end of the cage farthest from the test section opening, as seen in Fig. 3, ensures that the airfoil is as close to the aperture as possible.

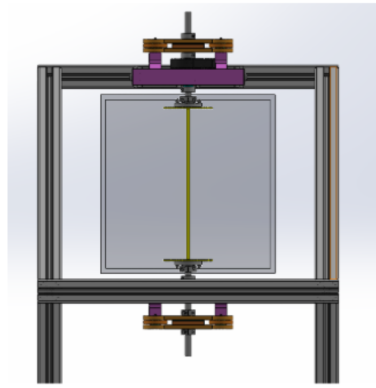

Fig. 5 Head-on view of apparatus. Span of the wing takes up majority of wind tunnel opening

D. Design of Pitch Degree of Freedom

In the pitch DOF, rotation from the wing must be transferred to the pitch springs. This is accomplished using a keyed shaft along with other keyed components. On either side of the wing is a keyed flanged shaft collar, shown in Fig. 6a. This collar is attached to the endplates of the wing using countersunk screws to keep the inner surface of the endplates smooth, as shown in Fig. 6b. Locknuts are used to secure the screws and prevent them from loosening during operation. A key is inserted into the keyseat of the shaft and the keyway of the shaft collar. As the wing pitches, the shaft collar will rotate, therefore rotating the shaft (Fig. 6c).

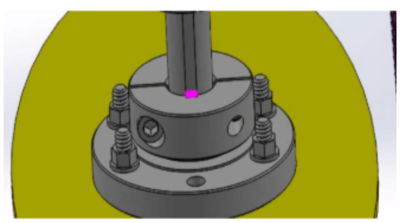

(a) The shaft collar attached to the endplate

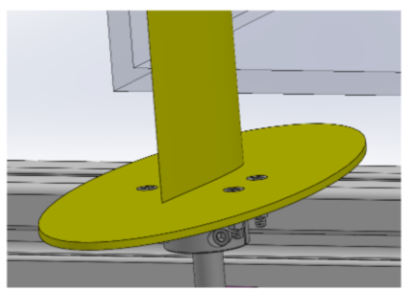

(b) Countersunk screws attach the shaft collar to the endplates of the wing, keeping the inner surface smooth.

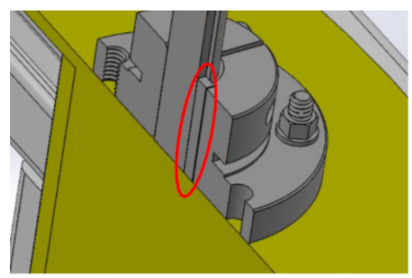

(c) The key which transfers rotation from the shaft collar to the shaft

Fig. 6 Shaft collar on the endplates of wing

The shaft runs through the wing heave mount. The purposes of this piece are to (1) attach the apparatus to the spring steel beams to support the heave degree of freedom and (2) provide a stationary surface to which the linear pitch springs can be mounted. This piece does not need to rotate with the shaft. Therefore, as shown in Fig. 7a and 7b, ball bearings were inserted on both sides of the piece. The central bore has a larger diameter than the shaft to prevent the shaft from rubbing against the wing heave mount. To attach the wing heave mount to the spring steel beams, a captive nut design is utilized, as shown in Fig. 8a and 8b. A slot, sized to the dimensions of the nut, was cut in the wing heave mount, ensuring the nut will remain in place despite any violent heaving the apparatus may endure. To aid with the durability of the apparatus, locknuts are used.

Shaft collars are used to keep the wing heave mount from moving vertically along the shaft. As shown in Fig. 9a, one side of the wing heave mount utilizes custom spacers that are placed between the inner race of the bearing and the shaft collar. As the shaft rotates, the inner race of the bearing and the shaft collar will also rotate, as will the spacer. This prevents friction between the bearing and shaft collar. On the other side of the wing heave mount, the optical encoder was mounted. To prevent friction between the encoder and the bearing, the bearing is placed in divot, as shown in Fig. 9b.

As the shaft rotates, so will the orange twister piece (refer to Fig. 10a). This is due to the key placed in the keyseat

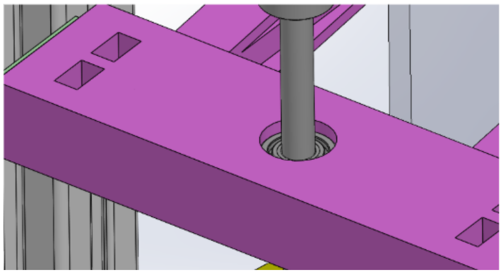

(a) Location of ball bearing on top of the wing heave mount

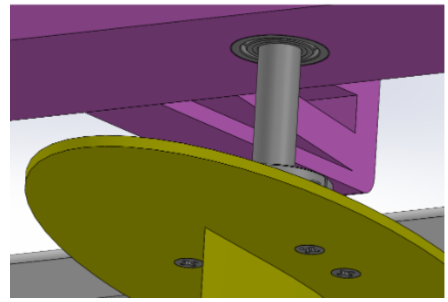

(b) Location of ball bearing on bottom of wing heave mount

Fig. 7 Location of ball bearings

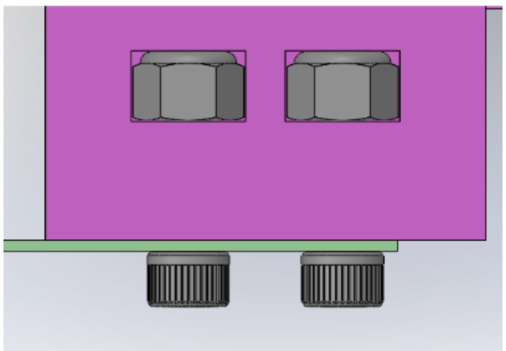

(a) Head on view of the captive nut slots

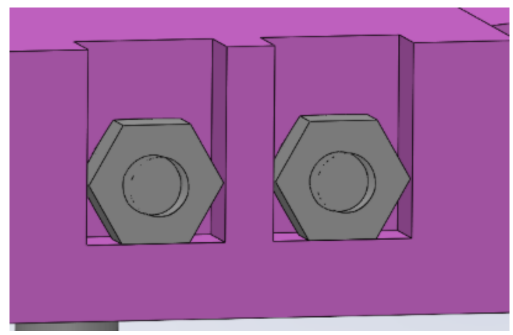

(b) Side view of captive nut slots

Fig. 8 Captive nut design

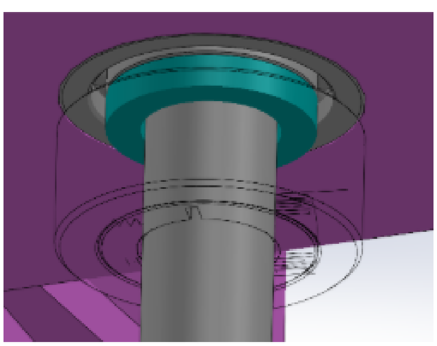

(a) Spacer placed in between inner race of bearing and shaft collar

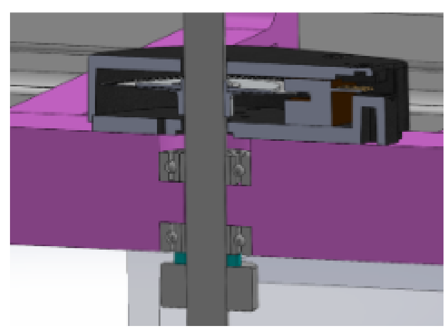

(b) Top bearing is placed in a divot to avoid contact with the encoder

Fig. 9 Spacer locations

of the shaft and the keyway of the twister, as shown in Fig. 10b.

As can be observed in Fig. 10a, j-hooks are attached to the twister. The j-hooks are used to mount the linear pitch springs; one end of the spring is attached to the j-hook on the twister and the other end is attached to the j-hook on the wing heave mount. Therefore, as the twister rotates, it will stretch one spring and compress the other, as shown in Fig. 11. It is important to note that even though one spring is compressed, it will still remain in tension because the springs are pre-tensioned. To allow for pre-tensioning, holes are drilled in the twister and through the mounting walls on the wing heave mount to allow for adjustment of the distance between j-hooks. Jam nuts are used on the j-hooks to prevent them from loosening as the apparatus oscillates.

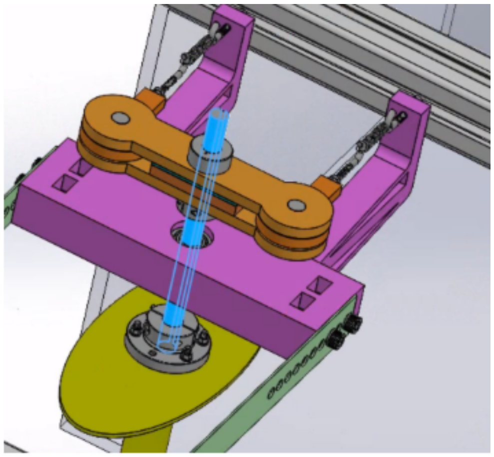

(a) Shaft runs through flanged shaft collar, wing heave mount, and orange twister.

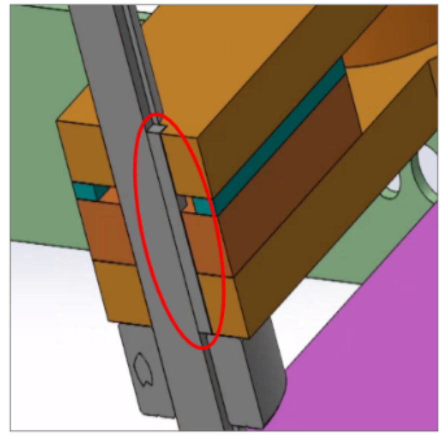

(b) Key placed between shaft and orange twister allows orange twister to rotate with the shaft

Fig. 10 Twister rotates with shaft

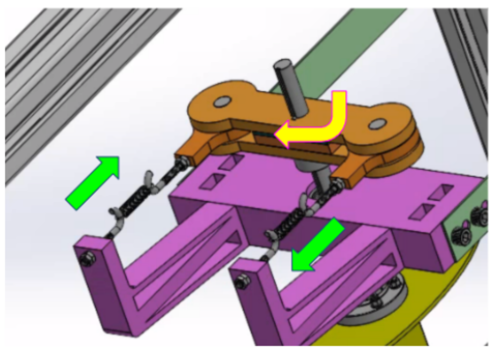

Fig. 11 Rotation of the twister (yellow arrow) will cause springs to stretch and compress (green arrows)

As the twister rotates, it is important that the pivot piece of the twister (to which the j-hooks are attached) can rotate independently so that the j-hooks on the twister can remain in line with the j-hooks on the wing heave mount. This is made possible through the design of the twister.

The twister is composed of three levels (each made up of separate pieces): a dogbone-shaped bottom, the middle pivot pieces, and a dogbone-shaped top (see Fig. 12a). On each side of the dogbone piece, there is a rod that runs from top to bottom. In the middle layer, a ball bearings are press-fitted in the pivot pieces, as shown in Fig. 12b. These bearings allow for the pivot pieces to rotate relative to the rod. During fabrication, the ends of the rods were epoxied to the outside faces of the dogbone pieces, preventing the rods from rotating relative to the twister.

The teal parts represent 3D-printed spacers that are used to reduce friction between the pivot and the dogbone pieces. As shown in Fig. 13, these spacers are placed on the inner race of the bearing to prevent the pivot pieces from being in direct contact with the dogbone pieces. Since the rod will never rotate relative to the twister, the inner race of the bearing will never rotate - only the outer race will be able to rotate. Since the outer race is pressed to the pivot piece, the pivot piece will be able to rotate.

This process is shown in Fig. 14. As the twister rotates (yellow arrow), the left rod will move backwards while the right rod will move forwards (green arrows). Since the pivot pieces can rotate independently, they will remain in line with the j-hooks on the wing heave mount (in line with the dotted red line in Fig. 14) instead of rotating with the rest of the twister.

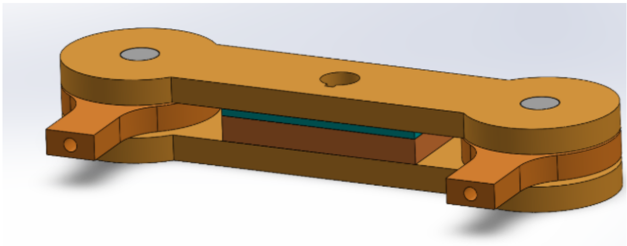

(a) Three levels of the twister

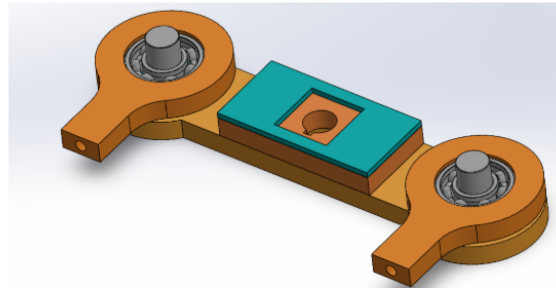

(b) Ball-bearings press-fit to the pivot piece. These bearings run through the epoxied rod.

Fig. 12 Design of twister

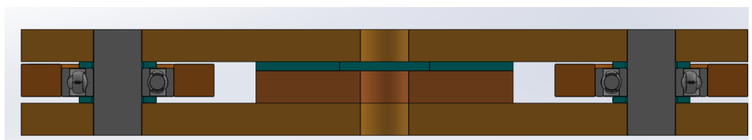

Fig. 13 Spacers (teal) are used to prevent contact between moving and stationary components

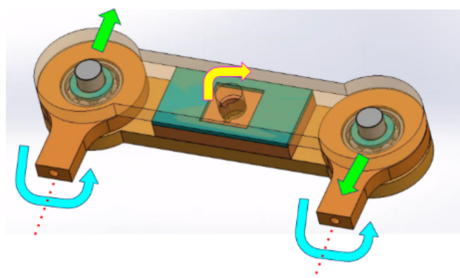

Fig. 14 As twister rotates, pivot pieces stay in line with the j-hooks mounted to the wing heave mount

E. Materials

To improve the durability of the apparatus, parts that use a key to transfer rotation from the airfoil were fabricated using metal instead of 3D printing. Consequently, the orange pieces of the twister (shown in Fig. 12a), namely the dogbone pieces and pivot pieces, were manufactured out of aluminum. Other pieces of the apparatus were 3D printed: the airfoil, custom spacers, and the wing heave mounts. Other items that couldn't be 3D printed or easily manufactured were ordered from external sources. Examples include the keyed shaft, flanged shaft collars, j-hooks, bearings, and key stock.

III. Results

A. Fabrication

The airfoil was 3D printed in one piece with both of the endplates. The first print was unsuccessful due to the lack of supports. As the airfoil got taller, vibrations from the printer would displace the airfoil, resulting in a very rough print and a loose connection with the top endplate. This was solved by adding a small fillet between the endplates and the wing as well as by adding additional support to the airfoil itself during the printing process.

To find the right size of 3D printed holes for screws, bearings, and nuts, test pieces were 3D printed with varying dimensions. Examples of these test pieces are shown in Fig. 15.

The aluminum pieces for the twister were cut from a sheet of 6.35 mm (0.25") aluminum using a waterjet. While the keyway on the dogbone pieces was sized correctly, the central hole of the pivot piece for which the bearing would be

Fig. 15 Test pieces used to size 3D printed bores

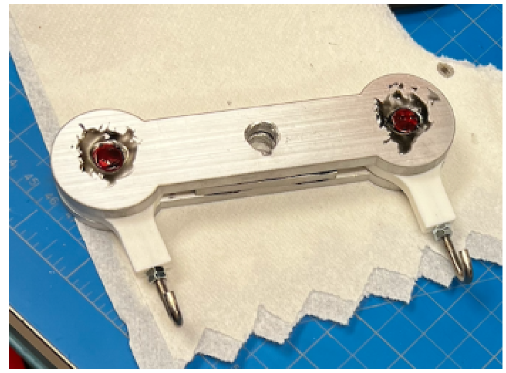

Fig. 16 Assembled twister

inserted was too small. As a result, when the bearings were press-fit into the aluminum pivot piece, the aluminum compressed the bearing, resulting in unsmooth rotation. Since these pivot pieces do not interface with keyed components, it was deemed appropriate to 3D print them. The 3D printed pivot pieces were successful, allowing for very smooth rotation, likely because the filament would make space for the bearing, so the balls in the bearing were not as compressed as they were in the aluminum piece. The assembled twister is shown in Fig. 16. Note the epoxy on the outer faces of the dogbone piece prevents the rod from rotating.

The outer cage was assembled using 80/20 aluminum extrusions and hardware. A circular saw was used to cut the extrusions to the correct lengths. The assembled cage is shown in Fig. 17.

The assembled apparatus is shown in Fig. 18.

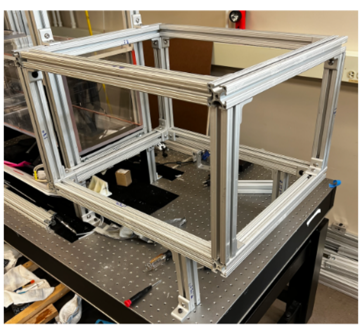

Fig. 17 Assembled cage

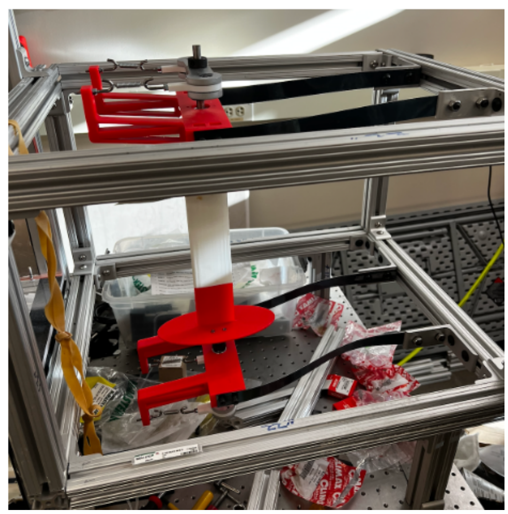

Fig. 18 Assembled apparatus

B. Evaluation

Assembly of the apparatus shows that the development of a two DOF apparatus is achievable in the small-scale wind tunnel. The goal of being able to easily mount and dismount the apparatus from the wind tunnel is achieved via the cage. The cage contains the entire apparatus within it, so the apparatus can be removed from the wind tunnel by simply dismounting the cage.

This apparatus is compatible with 3D printed airfoils, thanks to being able to mount the flanged collar to the endplates. The 3D printed airfoils, however, are extremely flexible because they are thin. Once the apparatus has been tested, it may be necessary to insert support rods through the airfoil to prevent it from twisting and buckling. Replacement of airfoils is also made possible by the flanged collars. To add a new airfoil, one can simply unscrew the old one from the flanged collars and then screw in the new one. This is especially important for the development of a neural network model because the network can now be exposed to different types of airfoils, not just one. Additionally, by having a second apparatus (the large-scale and small-scale versions), it is possible that the model could differentiate underlying patterns in the true dynamics of aeroelastic systems from noise unique to the environment of the apparatus.

Durability is addressed by using metal keyed parts. Additionally, locknuts are used throughout the apparatus (on the screws for mounting the wing to the flanged collar and on the screws that mount the spring steel beams to the wing heave mount) as well as jam nuts (where the j-hooks are attached to the pivot piece and wing heave mount).

After assembling the apparatus, it was discovered that the components (airfoil, wing heave mount, twister, hardware) attached to the spring steel beams are heavy enough to cause the beams to noticeably bend. Further work will address this challenge by implementing a support rail, on which rollers will be attached, so that the apparatus can frictionlessly heave while being supported.

Additionally, as can be observed in Fig. 18, the bottom spring steel beams buckle. This is likely because the holes each beam uses to attach to the wing heave mount are at slightly different distances from the end to which they mount to the cage. To fix this, the holes will be replaced with continuous slots, so that all the spring steel beams are attached at the same distance from the cage.

IV. Conclusion

This work detailed the development of a small-scale apparatus for LCO data collection designed to operate in the small-scale wind tunnel in the ISSRL lab at NCSU. The apparatus has two degrees-of-freedom: pitch and heave, which are measured by optical encoders and laser vibrometers, respectively. Stiffness in the pitch DOF is supported by linear springs and stiffness in the heave DOF is supported by spring steel beams. The design of the apparatus makes it compatible with 3D printed airfoils. Additionally, the use of flanged collars allows for easy substitution of airfoils, helping create a more diverse dataset on which a neural network model can be trained. Future work will focus on developing and implementing a rail to support the spring steel beams.

Acknowledgments

The authors thank Ryan Lynch for their contributions to the design and fabrication of the apparatus.

References

[1] Bisplinghoff, R., Ashley, H., and Halfman, R., *Aeroelasticity*, Dover Books on Aeronautical Engineering, Dover Publications, 2013. URL https://books.google.com/books?id=D1Gl4IWHjyUC.

[2] Garrick, I. E., and Reed, W. H., "Historical Development of Aircraft Flutter," *Journal of Aircraft*, Vol. 18, No. 11, 1981, pp. 897–912. https://doi.org/10.2514/3.57579, URL https://doi.org/10.2514/3.57579.

[3] Dowell, E., and Tang, D., *Nonlinear aeroelasticity and unsteady aerodynamics*, ???? https://doi.org/10.2514/6.2002-3, URL https://arc.aiaa.org/doi/abs/10.2514/6.2002-3.

[4] Dowell, E. H., *Nonlinear Aeroelasticity*, Springer International Publishing, Cham, 2022, pp. 489–533. https://doi.org/10.1007/978-3-030-74236-2_11, URL https://doi.org/10.1007/978-3-030-74236-2_11.

[5] Hughes, M. T., Gopalarathnam, A., and Bryant, M., "Automatic Limit Cycle Oscillation Annihilation in Aeroelastic Wings Using Prescribed Impinging Vortices," *AIAA Journal*, Vol. 64, No. 1, 2026, pp. 571–577. https://doi.org/10.2514/1.J065541, URL https://doi.org/10.2514/1.J065541.

[6] Jonsson, E., Riso, C., Lupp, C. A., Cesnik, C. E., Martins, J. R., and Epureanu, B. I., "Flutter and post-flutter constraints in aircraft design optimization," *Progress in Aerospace Sciences*, Vol. 109, 2019, p. 100537. https://doi.org/https://doi.org/10.1016/j.paerosci.2019.04.001, URL https://www.sciencedirect.com/science/article/pii/S0376042118301520.

[7] *Novel Active Control Strategy for LCO and Flutter Suppression by a Coordinated Use of Multiple Distributed Surface Actuators*, ASME International Mechanical Engineering Congress and Exposition, Vol. Volume 1: Advances in Aerospace Technology, 2014. https://doi.org/10.1115/IMECE2014-36905, URL https://doi.org/10.1115/IMECE2014-36905.

[8] Li, Q., Mei, C., and Huang, J.-K., "Suppression of Thermal Postbuckling and Nonlinear Panel Flutter Motions Using Piezoelectric Actuators," *AIAA Journal*, Vol. 45, No. 8, 2007, pp. 1861–1873. https://doi.org/10.2514/1.28280, URL https://doi.org/10.2514/1.28280.

[9] Hughes, M. T., Hall, D., Gopalarathnam, A., and Bryant, M., "Toward Active Control of Limit Cycle Oscillations in an Aeroelastic Wing Using a Variable Frequency Flow Disturbance Generator," *Nonlinear Structures & Systems, Volume 1*, edited by M. R. Brake, L. Renson, R. J. Kuether, and P. Tiso, Springer Nature Switzerland, Cham, 2024, pp. 205–213.

[10] Hall, D. A., Lynch, R. W., Hughes, M. T., Bryant, M., and Gopalarathnam, A., *Utilizing Machine Learning to Predict Limit Cycle Oscillation Characteristics in Aeroelastic Wing*, 2024.

[11] Kariv, D., Kunz, D. L., and Iovnovich, M., "Toward an Efficient Method for F-16 Limit Cycle Oscillation Prediction," *Journal of Aircraft*, Vol. 61, No. 2, 2024, pp. 558–569. https://doi.org/10.2514/1.C037391, URL https://doi.org/10.2514/1.C037391.

[12] Araujo, G. P., da Silva, J. A. I., and Marques, F. D., "Energy harvesting and passive mitigation from flutter via rotary nonlinear energy sink," *Journal of Sound and Vibration*, Vol. 603, 2025, p. 118953. https://doi.org/https://doi.org/10.1016/j.jsv.2025.118953, URL https://www.sciencedirect.com/science/article/pii/S0022460X25000276.

[13] Zipu Yan, Q. W. S. N. A., Honghua Dai, "Harmonic Balance Methods: A Review and Recent Developments," *Computer Modeling in Engineering & Sciences*, Vol. 137, No. 2, 2023, pp. 1419–1459. https://doi.org/10.32604/cmes.2023.028198, URL http://www.techscience.com/CMES/v137n2/53365.

[14] Raissi, M., Perdikaris, P., and Karniadakis, G., "Physics-informed neural networks: A deep learning framework for solving forward and inverse problems involving nonlinear partial differential equations," *Journal of Computational Physics*, Vol. 378, 2019, pp. 686–707. https://doi.org/https://doi.org/10.1016/j.jcp.2018.10.045, URL https://www.sciencedirect.com/science/article/pii/S0021999118307125.

[15] Visbal, M. R., and Garmann, D. J., *Numerical Investigation of Spanwise End Effects on Dynamic Stall of a Pitching NACA 0012 Wing*, 2017. https://doi.org/10.2514/6.2017-1481, URL https://arc.aiaa.org/doi/abs/10.2514/6.2017-1481.